Volume 15, Issue 1, 152505 (1-14)

Iranian Journal of Catalysis (IJC)

https://doi.org/10.57647/j.ijc.2025.1501.05

Synthesis, characterization and biological activity of Mn (II), Fe (II), Cd (II), and Hg (II) complexes using (benzo[d]thiazol-2-yldiazenyl)-4-nitroaniline as novel ligand in the epoxidation of alkenes under thermal and microwave irradiation

Jinan Mohsen Abdulrasool*

Al Sadder city Education, Al-Affa High School, Ministry of Education Baghdad, Baghdad, Iraq.

***Corresponding author:** jinanmohsen4@gmail.com

Original Research

Received:
26 June 2024
Revised:
30 October 2024
Accepted:
21 November 2024
Published online:
25 November 2024

Abstract:

Ligand formation in this research was accomplished by reacting each diazonium salt of 2-aminobenzothiazole with 4-nitroaniline. The ligand was characterized using various spectral techniques, including UV-Vis, FTIR, ^{1}H, and ^{13}CNMR, as well as LC-Mass. Furthermore, micro-elemental analysis (C.H.N.S.O) was conducted. Mn (II), Fe (II), Cd (II), and Hg (II) complexes were synthesized and thoroughly analyzed. The differentiation of metals in the chelates was determined through atomic absorption from flame, element analysis, infrared and UV-Vis spectral methods, and conductibility measurements to investigate their magnetic properties. The study provided insights into the molar ratio and continuous variation methods used to identify the compounds. Beer's law was utilized to determine the absorbance range (1×10^{-4} - 3×10^{-4} M/L), and complex solutions with high absorbability were observed. Analytical data for each chelated metal was reported in a 1:2 ratio of metallic ligand. The compounds displayed an octahedral geometry, as indicated by physico-chemical reference. Additionally, the biological activity of the compounds was evaluated. Moreover, for the practicality of these complexes, the Mn-complex was studied in the epoxidation of substituted styrene compounds as the target alkene to produce epoxide products.

Keywords: Alkene; Catalyst; Characterization; Epoxidation; Metal complex; Synthesis

1. Introduction

One of the primary obstacles in contemporary chemical synthesis is the substitution of economically and environmentally unsustainable techniques that require high energy consumption [1, 2]. The predominant use of stoichiometric atom inefficient oxidants, such as chromates, peracids, permanganates, and OsO4, in contemporary synthetic methods persists due to the significant challenge encountered [3, 4]. It is, in fact, this latter characteristic that positions the oxidation of 1st-row transition metals with O_2 and H_2O_2 at the forefront. This is especially true for systems that rely on titanium, copper, iron, and manganese. Epoxides play a crucial role as primary ingredients in the manufacturing of high-quality chemicals, including epoxy resins, surfactants, and paints, and serve as important building blocks in the field of organic synthesis [5]. The epoxidation of alkenes is a significant method for the production of epoxides and has garnered considerable interest from researchers [6–8]. Typically, the conventional methods employed in industrial processes include the chlorine-based non-catalytic process, co-epoxidation, and catalytic processes utilizing organic peroxides and peracids [9]. These techniques have long been established and widely adopted in various industrial applications. Nevertheless, these procedures are not cost-effective and require a significant amount of capital. Additionally, there are also environmental drawbacks that arise. The utilization of metal catalysts in the conversion of alkenes to epoxides using less harsh oxidants such as O_2, H_2O_2, and alkyl hydroperoxides has sparked signifi-

cant interest and led to the enhancement of exceptionally effective catalyst systems. Metal-based catalysts exhibiting high catalytic activity in metal-catalyzed epoxidations with alkyl hydroperoxides are characterized by possessing Lewis acidity and low oxidation potentials in their highest oxidation states. The order of activity among these catalysts is as follows: Mo > W > Ti > V [10, 11].

The advancement of environmentally friendly techniques for catalyzing the oxidation of alkene compounds presents a crucial scientific obstacle with substantial technological promise [12–14]. Specifically, the epoxidation of alkenes stands out as a significant reaction due to its ability to convert basic hydrocarbon materials into valuable, high-quality chemical products. Furthermore, there is an added stress that for the technological capabilities of the chemistries to be actualized in an industrial environment, they need to be eco-friendly, utilize atom-efficient and non-harmful reagents, and must function under gentle circumstances.

Over the past twenty years, there has been significant interest in metal complex catalysts that contain ligands with Nitrogen donor atoms [15–19]. These catalysts have gained attention due to their wide range of applications in organic synthesis and catalysis, both in industrial and academic settings [20, 21]. Within the human body, the Cytochrome P-450 enzyme plays a crucial role in selectively oxidizing the incorporation of an O atom into numerous substrates during various bioorganic reactions [22, 23]. Notably, several research groups have recently synthesized diverse metal complex catalysts that exhibit similar performance to the Cytochrome P-450 enzyme. Transition metal complexes have been recognized for their efficacy as organometallic catalysts in the epoxidation of alkenes using $NaIO_4$, NaClO, H_2O_2, $KHSO_5$, and PhIO as sources of single-atom oxygen [24–27]. However, the catalytic performance of these complexes has been hindered by the deactivation of metals and their subsequent leaching into the reaction medium.

Microwave irradiation has gained recognition as a multifaceted technology with substantial applications in diverse domains, such as wastewater treatment, biological studies, construction materials, agriculture, and the synthesis of nanomaterials and organic compounds [28, 29]. This technique employs electromagnetic waves to generate both thermal and non-thermal effects, resulting in modifications to material characteristics and biological interactions. The growing interest in microwave technology stems from its ability to improve the efficiency and effectiveness of processes that have traditionally depended on chemical or thermal approaches. This introduction will examine the wide-ranging applications of microwave irradiation, emphasizing its significance in environmental management, biological processes, materials science, agricultural methodologies, and nanotechnology. Several organic transformations have been conducted using microwave irradiation, demonstrating benefits such as high yields and reduced reaction times [30–34].

In this study, a novel ligand was synthesized, followed by the preparation of a range of organometallic catalysts incorporating Mn, Fe, Cd, and Hg. These catalysts were designed to facilitate the efficient epoxidation of alkenes using sodium periodate as the oxidizing agent under thermal and microwave irradiations.

2. Experimental

2.1 General

The chemicals and solvents employed in this investigation are of analytical quality and do not require further purification. These include $MnCl_2.4H_2O$, $FeCl_2$, $CdCl_2.H_2O$, and $HgCl_2$ (Fluka), 2-aminobenzothiazole, and 4-nitroaniline (B.D.H). The Brucker-300 MHz Ultra Shield spectrometer at Al-al-Bayt University was utilized to obtain the ^{13}C and ^{1}H-NMR spectra. The solvent used for these experiments was $(CH_3)_2SO$, with tetramethylsilane serving as the reference compound. At the University of Damascus, a Euro vector A single V.3.O EA 3000 instrument was employed to conduct a microanalysis of the elements (C.H.N.S.O). The conductivity test of the complexes dissolved in DMSO (10^{-3} M/L) was carried out at 25 °C using a Philips PW-Digital Conductometer. Magnetic characteristics were determined at 25 °C using the Auto Magnetic Susceptibility Balance Sherwood Scientific tool in conjunction with the Shimadzu A.A-160A Atomic Absorption/Flame Emission Spectrophotometer. The UV-visible spectral data were recorded using a Spectrophotometer with Ultraviolet and Visible Light UV-160A Shimadzu. Infrared (IR) spectral data were collected using a Shimadzu FTIR-8400S Fourier Transform Infrared Spectrophotometer, covering the range of $4000 - 400$ cm^{-1}. The spectral patterns were obtained by producing KBr discs. The mass spectra were acquired using the LC-MS QP5OA: Shimadzu (E170 EV) Spectrometer at Dimashq University, Syria. Finally, the melting points were determined using the Stuart Melting Point Apparatus.

2.2 Preparation of azo ligand

A 0.375 g (1 mmol) solution of 2-aminobenzothiazole was prepared in a mixture of 10 mL ethyl alcohol and 2 mL concentrated hydrochloric acid. This solution was then diazotized at 5 °C using a 10% solution of $NaNO_2$. The diazotized solution was slowly added to a cooled ethyl alcohol solution (0.345 g, 1 mmol) containing 4-nitroaniline with stirring. Subsequently, a NaOH solution was mixed into the resulting dark-colored mixture, leading to the precipitation of the azo ligand. The precipitate was washed multiple times with a 1:1 mixture of ethyl alcohol and water and then dried [35].

2.3 Preparation of buffer and standard solution

The buffer solution was prepared by dissolving 0.771 grams of ammonium acetate (0.01 M) in one liter of doubly deionized water. Subsequently, the pH range of the solution was adjusted to 4-9 using either acetic acid or an ammonia solution. Two sets of solutions containing metallic salts with varying concentrations ($10^{-5} - 10^{-3}$ M/L) were meticulously prepared within a pH range of 4 to 9. Additionally, a substantial quantity of ethanol originating from ligands underwent condensation reactions, resulting in solutions with concentrations ranging from 10^{-5} to 10^{-3} M/L.

2.4 Preparation of metal complexes

An ethanolic solution containing 0.299 g and 2 mmol of azo ligand (L) was slowly added dropwise to a stirred solution composed of 0.099 g, 0.063 g, 0.100 g, and 0.136 g of $MnCl_2.4H_2O$, $FeCl_2$, $CdCl_2.H_2O$, and $HgCl_2$, respectively. The pH of the solution was adjusted to the desired level. The mixture was stirred until a dark color precipitate formed, which was then collected, filtered, and washed multiple times with a 1:1 mixture of H_2O and C_2H_5OH.

2.5 Antimicrobial activity of metal complexes

The ligand, along with all the synthesized compounds, was assessed for its in vitro antibacterial efficacy against *Staphylococcus aureus*, *Staphylococcus epidermidis*, and *Pseudomonas Aeruginaso*, as well as its antifungal efficacy against *Candida albicans (Yeast)*, using the disk diffusion method. The active test samples were dissolved in DMSO, and concentrations ranging from 1 to 200 μg/ml were used. The antibacterial and antifungal activities of each compound were evaluated using the well-diffusion method. A volume of 1 cm^3 of a 24-hour broth culture containing 106 CFU/cm^3 of gram-negative bacteria (*Streptococcus sp., Escherichia coli, and Klebsiella sp.*) was placed on sterilized Petri dishes. Molten nutrient agar (15 cm^3) was kept at approximately 45 °C and poured into the Petri dishes to solidify. Using a sterilized cork borer, carefully punctured holes with a diameter of 6 mm were made, and these holes were completely filled with the assay solutions. The dishes were then incubated at 37 °C for 24 hours [36].

2.6 Typical procedure for the epoxidation of substituted styrenes using Mn-complex under thermal conditions

In a 25 mL flask containing a condenser and a magnetic stirring bar, a solution of alkene (5.0 mmol), sodium periodate (5.0 mmol), and Mn-complex (250 mg) in 10 mL of H_2O: CH_3CH_2OH (2:1) was heated under reflux conditions. The reaction progress was tracked using gas chromatography. Upon finishing the reaction, the complexes were separated by filtration and rinsed with chloroform and dichloromethane (15 mL). The resulting product was then subjected to purification on a silica-gel plate to obtain the pure compound.

2.7 The reusability of the catalyst under thermal conditions

The potential for reusing the Mn-catalyst was examined through a series of consecutive epoxidation reactions involving 4-hydroxystyrene. Following each reaction, the catalyst was isolated from the reaction mixture via straightforward filtration, subsequently washed with a mixture of diethyl ether and chloroform, and then dried in preparation for its application in the subsequent reaction cycle.

2.8 Microwave irradiations for the epoxidation of alkenes

A mixture consisting of alkene (2.0 mmol), sodium periodate (2.0 mmol), and a manganese complex (100 mg/ 1 mol%) dissolved in 10 mL of dichloromethane was stirred for one hour in a beaker. Subsequently, this vigorously stirred solution was transferred to a long-neck open vessel and subjected to microwave irradiation at a temperature of 70 °C and a power setting of 250 W. Upon concluding the reaction observed through gas chromatography, the phases were segregated, followed by the evaporation of the organic layer. The crude product underwent purification utilizing chloroform and dichloromethane (15 mL). Subsequently, the resultant product was further purified on a silica-gel plate to isolate the pure compound.

3. Results and discussion

3.1 Synthesis and characterization of azo ligand and metal complexes

The azo ligand derived from 4-nitroaniline was synthesized to create a diazotized alkaline solution (Scheme 1). Through spectral analysis, the synthesized azo ligand was characterized using various techniques such as ^{13}C and ^{1}H NMR, FT-IR, UV-UV-visible, LC-Mass, and micro-elemental analysis (C.H.N.S.O). The interaction of metal salts with the synthesized ligand yielded the desired product from aqueous ethyl alcohol solutions, which was then used for further investigation.

Ligands in ^{1}HNMR spectra exhibit a range of signals between δ= 6.610 – 8.300 ppm, corresponding to aromatic protons. Notably, signals at δ= 8.449 ppm and δ= 2.50 ppm are attributed to δ (NH_2) and DMSO-d_6, respectively, as illustrated in Figure 1a [37]. On the other hand, in ^{13}CNMR spectra, ligands resonate at δ=149.960 ppm, indicative of carbon in the amino group [38]. Additionally, a variety of signals at δ=151.591, δ=143.039, δ=132.192, δ=130.739, δ=126.346, δ=126.257, δ=125.348, δ=124.672, δ=124.011, δ=123.043, δ=121.721, and δ=120.802 ppm are associated with carbon atoms in aromatic rings [39, 40]. The signal at δ=39.751 ppm is attributed to DMSO-d_6, as shown in Figure 1b.

The concentrated peak observed at m/z = 299 in the mass spectrum of the Ligand, which was prepared from azo (L), can be attributed to the presence of the $C_{13}H_9N_5O_2S$ formulation. The overall fragmentation pattern of the Ligand is summarized in Scheme 2, as depicted in Figure 2.

A solution containing an azo ligand dissolved in ethanol was carefully dripped into a solution containing $MnCl_2.4H_2O$, $FeCl_2$, $CdCl_2.H_2O$, and $HgCl_2$ while being stirred. The pH of the solution was adjusted to the desired value. The resulting mixture was continuously stirred until a dark-colored precipitate formed. This precipitate was

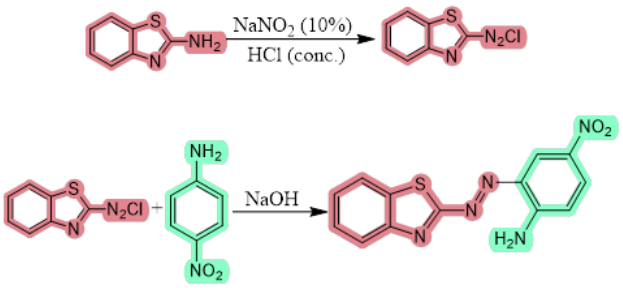

Scheme 1. Synthesis of azo Ligand.

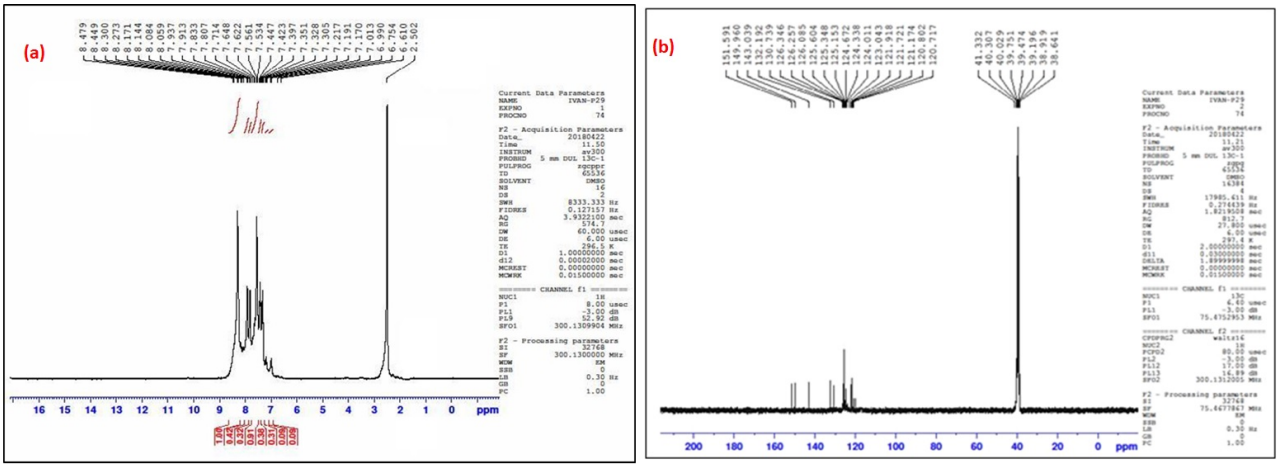

Figure 1. ^{1}H NMR and ^{13}CNMR of azo Ligand.

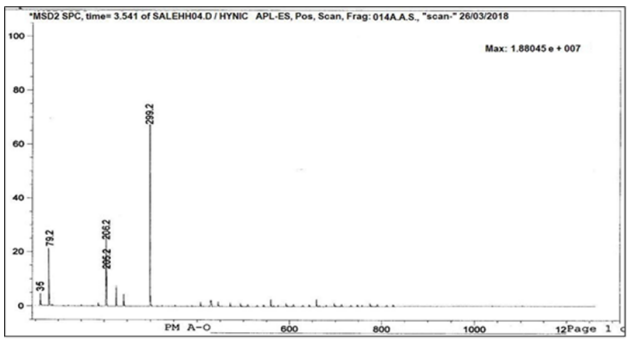

Figure 2. Mass spectra of Ligand.

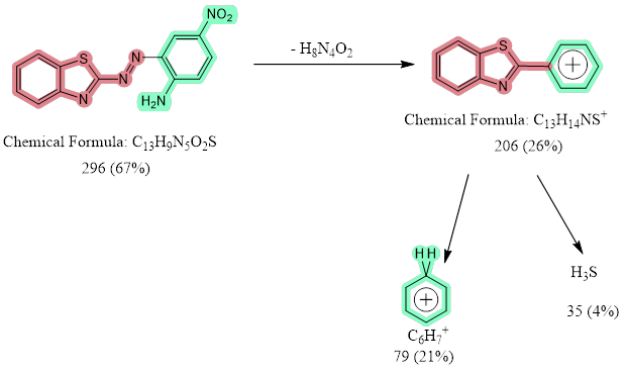

Scheme 2. Ligand fragmentation.

subsequently collected, filtered, and subjected to multiple washes using a mixture of H_2O and C_2H_5OH in a 1:1 ratio. The chemical structures of the metal complexes can be observed in Figure 3.

The synthesized ligand and metal complexes, which included Mn, Fe, Cd, and Hg, underwent physical and elemental analysis. The results, such as melting point, yield, color, and CHN analyzer data, were organized in Table 1.

The UV-visible spectra of dissolved compounds prepared in ethyl alcohol ($10-3$ M/L) were measured, and the resulting data is documented in Table 2. The UV-visible spectrum of the azo ligand displays peaks at 218, 290, and 410 nm, which correspond to energy transitions ($\pi-\pi^*$) [41]. The Mn (II) spectrum exhibits three peaks at 223, 301, and 445 nm due to intra-ligand and charge transfer processes [42]. Peaks at 543 and 681 nm are assigned to electronic transitions of 6 Aig$\rightarrow$ 4 A_{1g}, #Eg (G) and 6 Aig$\rightarrow$ $^{4}T_{2g}$, #Eg (G), respectively [43]. The magnetic moment value of the compound is 5.72 B.M, indicating a close resemblance to an octahedral environment. The Fe (II) spectrum shows peaks at 220, 311, and 431 nm, which are attributed to ligand field and charge transfer effects. Another peak at 547 nm corresponds to the electronic transition type $^{5}T_{2g}\rightarrow$ ^{5}Eg, with a magnetic moment value of 4.81 B.M supporting the octahedral geometry. The electronic spectra of Cd (II) and Hg (II) complexes demonstrate charge transfer, and the absence of magnetic susceptibility in diamagnetic compounds suggests that (d-d)

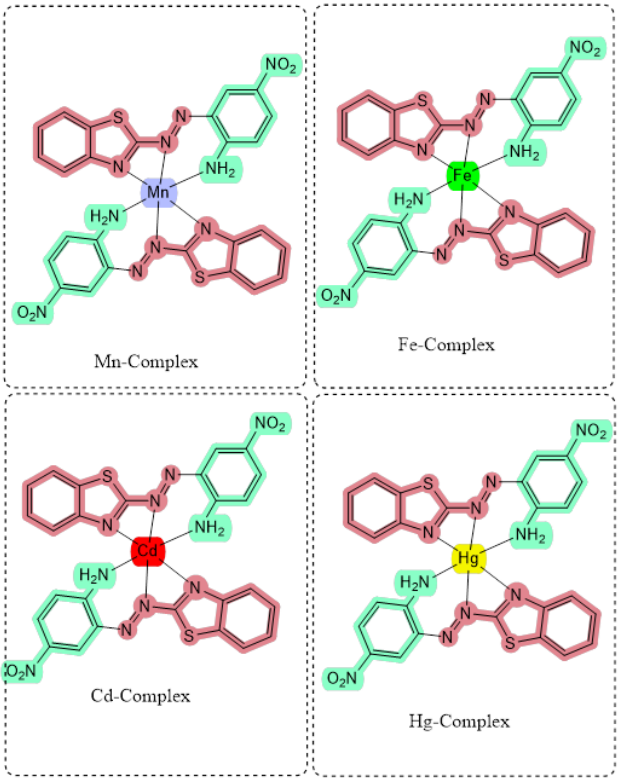

Figure 3. The chemical structure of metal complexes.

Table 1. Physical estates for azo ligand as well as metal compounds.

Entry	Compounds	Color	M.P (°C)	Yield (%)	Analysis Calc (Found)					
					M (%)	C (%)	H (%)	N (%)	O (%)	S (%)
1	Ligand (L)	Brown	201 – 203	81	-	52.17 (51.94)	3.01 (2.45)	23.41 (22.27)	10.70 (9.01)	10.70 (9.23)
2	$[Mn(L)_2]Cl_2$	Reddish Brown	243 – 245	85	7.59 (6.91)	43.09 (42.92)	2.48 (2.11)	19.33 (18.77)	8.83 (7.89)	8.83 (7.94)
3	$[Fe(L)_2]Cl_2$	Deep brown	262 – 264	80	7.72 (6.92)	43.03 (42.96)	2.48 (2.06)	19.31 (18.88)	8.82 (7.78)	8.82 (7.86)
4	$[Cd(L)_2]Cl_2$	Red	251 – 253	82	14.34 (13.88)	39.94 (38.84)	2.30 (2.02)	17.92 (16.81)	8.19 (7.68)	8.19 (7.94)
5	$[Hg(L)_2]Cl_2$	Reddish brown	273 – 275	86	23.10 (22.75)	35.86 (34.76)	2.06 (2.12)	16.09 (15.93)	7.35 (6.81)	7.35 (6.85)

Table 2. Conditions from produced complexes as well as UV-visible, magnetic susceptibility and conductance mensuration's data.

Entry	Compounds	Optimum pH	Optimum Molar Conc.$\times 10^{-4}$	M:L Ratio	λ_{max} (nm)	ABS	ε_{max} (L/molcm)	Λ_m (Scm^2/mol) in DMSO	μ_{eff} (B.M)
1	Ligand(L)	-	-	-	218 290 410	2.198 0.780 2.340	2198 0.785 2.340	-	-
2	$[Mn(L)_2]Cl_2$	7	2.0	1:2	223 301 445 543 681	2.025 0.995 0.631 0.052 0.033	2025 995 631 52 33	71.62	5.72
3	$[Fe(L)_2]Cl_2$	7	2.5	1:2	220 311 431 533	1.974 1.955 0.583 0.077	1974 1955 583 77	76.18	4.81
4	$[Cd(L)_2]Cl_2$	7	2.5	1:2	225 321 477	2.117 0.873 0.447	2117 873 447	76.63	Dia
5	$[Hg(L)_2]Cl_2$	7	2.0	1:2	227 311 472	2.372 0.952 0.396	2372 952 396	79.30	Dia

transitions are unlikely, hence no data was obtained from the electronic spectra. This observation aligns well with previous studies on octahedral complexes (Figure 4).

The chelation ratio was (1:2) (Metal: Ligand) and was formed through the interaction of the ligand dissolved in ethyl alcohol with metal ions at the optimal pH. The results obtained from elemental analysis, as well as the metal content of the compounds, have been found to be in close agreement with the calculated values. The conductivity of the chelates formed by the molten metal in dimethylsulfoxide ($10-3$ M/L) shows an electrolytic species ratio of (1:2), with detailed data provided in Table 2. Different molar condensation (10^{-5}–10^{-3} M/L) was observed when a ligand consisting of a mixture of aqueous ethyl alcohol and metal ions was used. The resulting condensation, which amounted to ($10^{-3}\times 10^{-4}$ M/L), followed Beer's law and displayed a distinct and vibrant color. The binding factor was determined by fitting the data to the best straight lines, with a correlation coefficient (R) greater than 0.9980, as shown in Figure 5.

To explore the connection between the bonding interactions and metal ions in educational contexts during the formation

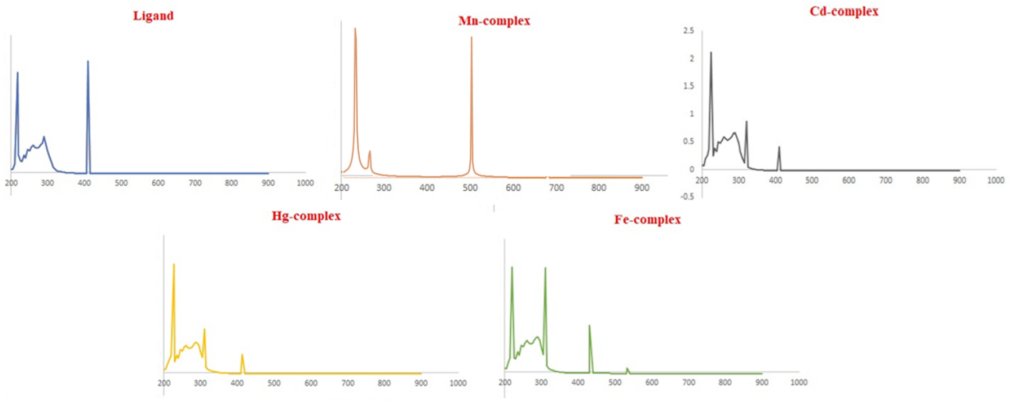

Figure 4. UV-Vis spectra of ligand, and synthesized metal complexes.

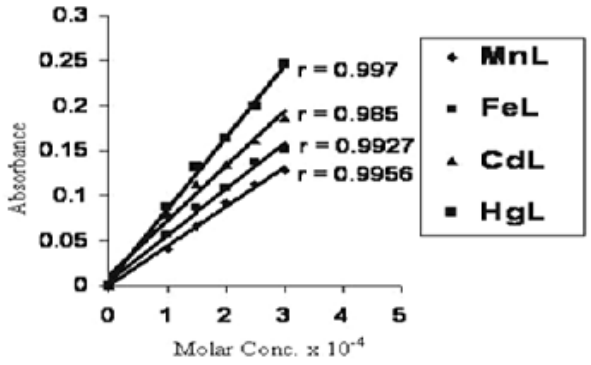

Figure 5. Linear relationship between absorption as well as molar concentration.

of complexes, spectrophotometry was employed to combine ligand solutions with metal ions at the optimal pH, using a predetermined wavelength (λ_{max}) as the initial procedure. The mole ratio of metal to ligand (M: L) was used to define the prepared complexes. The optimal concentration was determined by selecting the complex solution that exhibited the highest absorption at a constant wavelength (λ_{max}) across different pH levels. Furthermore, the experiment results, as shown in Table 2, confirmed the sorption capacity of each prepared complex, which remained stable in a buffer solution of NH_4OOCCH_3 within the pH range of $4-9$. All prepared complexes displayed a consistent pH profile, as depicted in Figure 6.

The complexes present in the solutions were evaluated through the analysis of the mole ratio and the technical aspects of the pointed test. In each scenario, the findings will be reported as a 1:2 ratio (metal to ligand). The graph chosen for display can be found in Figure 7, while the detailed data is presented in Table 2. The outcomes were consolidated and further analyzed for the specific characteristics of the complexes.

Table 3 contains the registered data of FT-IR for Azo ligands and their complexes. The spectral bands of the ligands were observed at 3484 cm^{-1} and 3414 cm^{-1}, indicating both asymmetric and symmetric frequencies of the υ (NH_2) group. In the spectra of all the synthesized compounds, these bands were found to shift to lower frequencies due to coordination with the ionic metal. Another band at 1639 cm^{-1}, assigned to the υ (C=N) group,

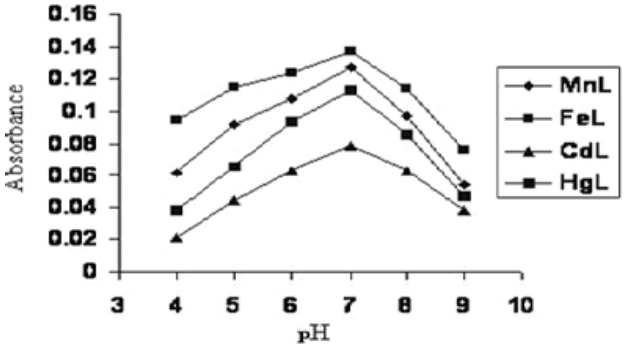

Figure 6. Effect from pH in absorption (λ_{max}) with metal chelates.

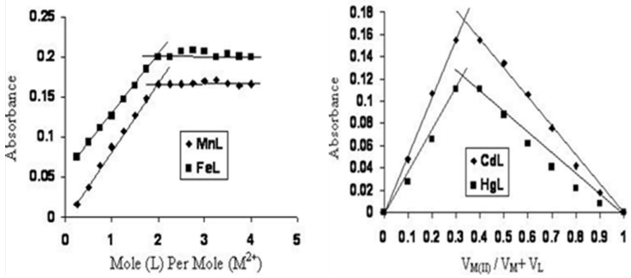

Figure 7. Molar ratio as well as working methods for solutions of compounds.

was observed to have a lower frequency, confirming the coordination of the ionic metal. Additionally, vibrations from the υ (C=C) group were represented by bands at 1593 cm^{-1} and 1562 cm^{-1}, while the band at 1446 cm^{-1} indicated a lower wavenumber for the υ (N=N) frequency, accompanied by changes in the spectrum shape for all the prepared complexes. The frequency bands extending to the metal-nitrogen bond were more pronounced, falling within the range of $424-486$ cm^{-1} [44].

3.2 Computational study of complexes

Contemporary theoretical electronic structure techniques, especially those utilizing density functional theory (DFT), enable easy optimization of molecular geometries and computation of various molecular properties. The analysis of energy minimization, molecular orbital, atom dots map representation, and model axes or view axes of metal complexes of azo ligand, specifically Mn-complex, Fe-complex, Cd-complex, and Hg-complex, involved the process of modelling and geometry optimization. This study was conducted, and the findings are presented in Figures 8-11, and Tables 4-7.

3.3 Antimicrobial screening of azo ligand and metal complexes

The antibacterial and antifungal efficiencies of the ligand prepared from azo (L) and the recorded compounds were evaluated against *Staphylococcus aureus, Staphylococcus epidermis, Pseudomonas Aeruginaso* (G^{+ev}), *Streptococcus*

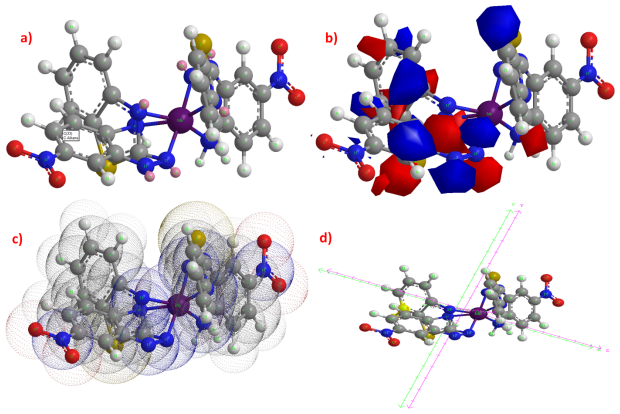

Figure 8. DFT calculation of Mn-complex a) optimized structure b) Molecular orbital c) atom dots representation d) view axes (pink line) and model axes (green line).

Table 3. Characteristic frequencies for azo ligand and metal chelates.

Entry	Compounds	υ(NH_2)	υ(C=N)	υ(C=C)+υ(N=N)	υ(M-N)
1	Ligand (L)	3484 s. 3414 sh.	1639 sh.	1593 sh. 1562 sh. 1446 s.	None
2	$[Mn(L)_2]Cl_2$	3381 sh. 3366 sho.	1620 s.	1593 sh. 1560 sho. 1427 sh.	480 w. 471 w.
3	$[Fe(L)_2]Cl_2$	3390 s. 3382 sh.	1627 sh.	1592 sh. 1561 sho. 1427 sh.	450 w. 422 w.
4	$[Cd(L)_2]Cl_2$	3385 sh. 3370 sho.	1625 sh.	1593 sh. 1560 sho. 1425 s.	472 w. 461 w.
5	$[Hg(L)_2]Cl_2$	3375 s. 3362 sho.	1626 sh.	1595 sh. 1558 sh. 1427 s.	462 w. 440 w.

Sharp: Sh.; Strong: S.; Shoulder: Sho.; Weak: W.

Table 4. The valuable data using DFT calculation for Mn-complex.

Stretch	Bend	Stretch-Bend	Torsion	Non-1,4 VDW	1,4 VDW	Charge/Charge	Charge/Dipole	Total Energy
374.9	275.5	-14.3	147.9	285.7	262.1	0.0907	2.597	1334.6 kcal/mol

Table 5. The valuable data using DFT calculation for Fe-complex.

Stretch	Bend	Stretch-Bend	Torsion	Non-1,4 VDW	1,4 VDW	Charge/Charge	Charge/Dipole	Dipole/Dipole	Total Energy
25.9	218.5	-7.3	107.6	-10.7	52.8	264.9	4.9	3.6	660.2 kcal/mol

Table 6. The valuable data using DFT calculation for Cd-complex.

Stretch	Bend	Stretch-Bend	Torsion	Non-1,4 VDW	1,4 VDW	Charge/Charge	Charge/Dipole	Dipole/Dipole	Total Energy
5.93	110.7	-2.8	159.1	-16.5	43.9	0.17	2.3	4.75	307.6 kcal/mol

Table 7. The valuable data using DFT calculation for Hg-complex.

Stretch	Bend	Stretch-Bend	Torsion	Non-1,4 VDW	1,4 VDW	Charge/Charge	Charge/Dipole	Dipole/Dipole	Total Energy
6.1	117.8	-2.87	151.7	-16.7	44.8	0.10	2.6	6.14	309.6 kcal/mol

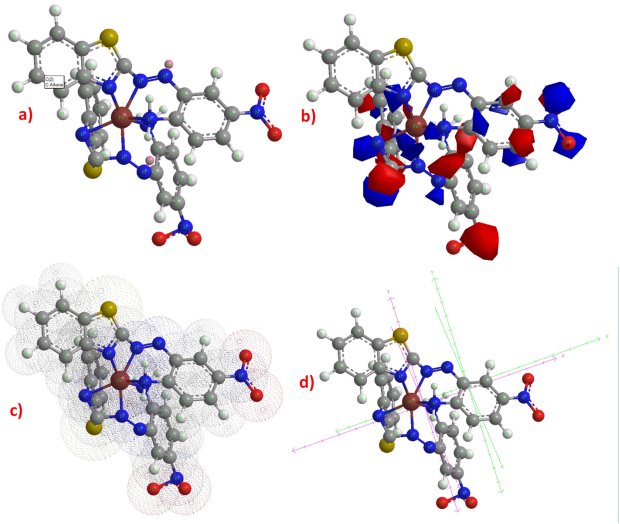

Figure 9. DFT calculation of Fe-complex a) optimized structure b) Molecular orbital c) atom dots representation d) view axes (pink line) and model axes (green line).

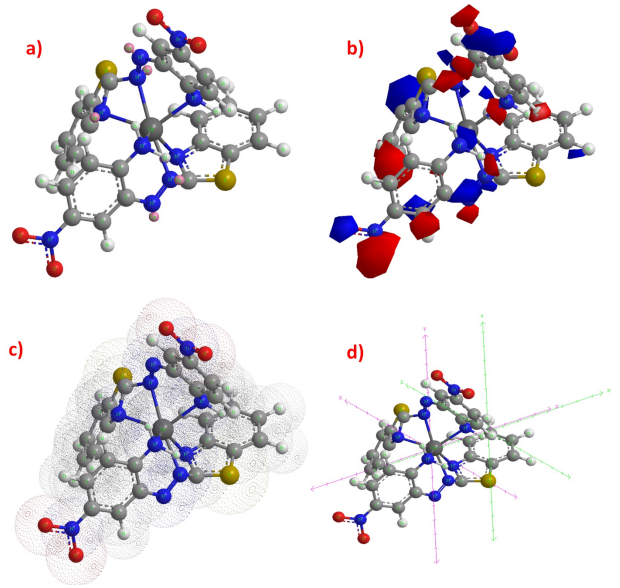

Figure 10. DFT calculation of Cd-complex a) optimized structure b) Molecular orbital c) atom dots representation d) view axes (pink line) and model axes (green line).

sp., Escherichia coli, Klebsiella sp. (G^{-ev}), and *Candida albicans (Yeast)* using the disk diffusion method. The zone inhibition data for the ligand and complexes are presented in Table 8, indicating the measured millimeters of inhibition. Among all the complexes, significant antibacterial and

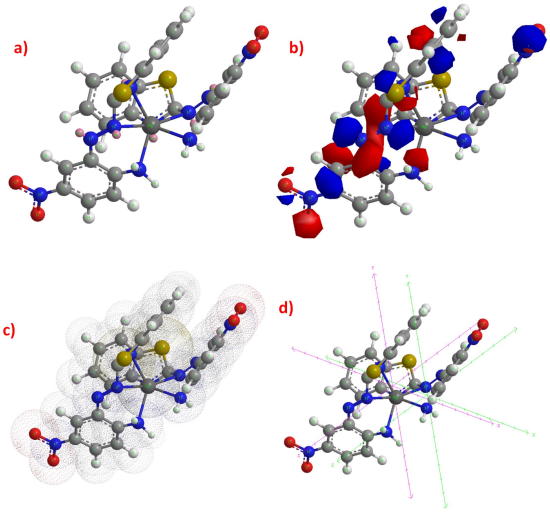

Figure 11. DFT calculation of Hg-complex a) optimized structure b) Molecular orbital c) atom dots representation d) view axes (pink line) and model axes (green line).

antifungal activities were observed.

3.4 Catalytic evaluation of Mn-complex

Following the preparation, characterization, and DFT calculation of the ligand and metal complexes, the optimization of reaction conditions for the epoxidation of styrene was conducted. Sodium periodate was chosen as the oxidant, and a Mn-complex was used as the catalyst. The aim was to determine the ideal solvent, oxidant, and catalyst amount for the reaction. To begin, the model reaction was carried out using various solvents, including CH_3CN, water, methanol, ethanol, and different ratios of water with $C_2H_5OH/CH_3OH/CH_3CN$. The results, as presented in Table 9 entries $1-10$, indicated that the most efficient medium for the reaction was a mixture of water and C_2H_5OH in a 2:1 ratio. Next, different oxidants were tested for the model reaction, including $NaIO_4$, H_2O_2, NaOCl, and tert-butOOH. From the experiments detailed in Table 5 entries $11-13$, $NaIO4_4$ was identified as the most effective oxidant. Furthermore, the catalytic amount of the Mn-complex was investigated. Table 9 entries $14-15$ revealed that 250 mg of the Mn-complex was determined to be the optimal catalyst amount. In summary, the optimization process involved the selection of the most suitable solvent, oxidant, and catalyst amount for the epoxidation of styrene. The results indicated that a mixture of water and C_2H_5OH (2:1) served as the ideal medium, $NaIO_4$ was the preferred oxidant, and 250

Table 8. Biological efficacy results for azo ligand (L) as well as complexes offered the inhibition circle diameter at millimeters with the bacteria after 24h.

Compounds	*Staphyl- ococcus aureus* (G^{+ev})	*Staphyloco- ccus epidermidis* (G^{+ev})	*Psedomonas Aeruginaso* (G^{+ev})	*Steptococcus sp.* (G^{-ev})	*Escherichia coli* (G^{-ev})	*Klebsiella sp.* (G^{-ev})	*Candida albicans (Yeast)*
Control (DMSO)	-	-	-	-	-	-	-
Ligand(L)	10	12	11	11	10	10	9
$[Mn(L)_2]Cl_2$	12	10	10	11	11	11	10
$[Fe(L)_2]Cl_2$	13	8	10	12	8	10	8
$[Cd(L)_2]Cl_2$	12	10	11	10	10	11	11
$[Hg(L)_2]Cl_2$	14	14	12	14	14	12	17
Cefazoline (30 μg/g)	18	15	14	12	14	18	-

Table 9. Optimization of the model reaction conditions[a].

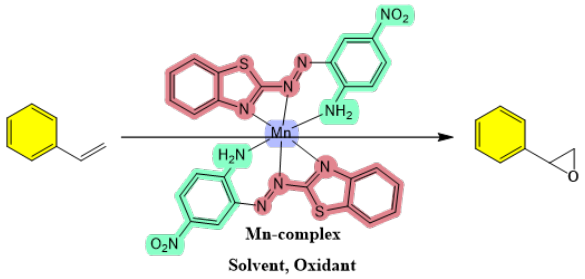

Entry	Oxidant	Solvent	Catalyst amount (mg)	Time (h)	Yield (%)[b]
1	$NaIO_4$	H_2O	250	3.5	63
2	$NaIO_4$	CH_3CN	250	3.5	59
3	$NaIO_4$	CH_3CH_2OH	250	3.5	48
4	$NaIO_4$	CH_3OH	250	3.5	55
5	$NaIO_4$	H_2O/ CH_3CN (1:1)	250	3.5	71
6	$NaIO_4$	H_2O/ CH_3CN (2:1)	250	3.5	73
7	$NaIO_4$	H_2O/ CH_3CH_2OH (1:1)	250	3.5	75
8	$NaIO_4$	H_2O/ CH_3CH_2OH (2:1)	250	3.5	87
9	$NaIO_4$	H_2O/ CH_3OH (1:1)	250	3.5	56
10	$NaIO_4$	H_2O/ CH_3OH (2:1)	250	3.5	60
11	H_2O_2	H_2O/ CH_3CH_2OH (2:1)	250	5.5	49
12	NaOCl	H_2O/ CH_3CH_2OH (2:1)	250	5.5	56
13	tert-ButOOH	H_2O/ CH_3CH_2OH (2:1)	250	5.5	53
14	$NaIO_4$	H_2O/ CH_3CH_2OH (2:1)	200	4.5	80
15	$NaIO_4$	H_2O/ CH_3CH_2OH (2:1)	300	2.5	86
16	$NaIO_4$	H_2O/ CH_3CH_2OH (2:1)	-	10	20 (35)[c]

a) Reaction conditions: $C_6H_5CH{=}CH_2$ (5 mmol), oxidant (5 mmol), Solvent (10 mL).Room temperature b) GC Yields. c) The reaction was performed under air for providing oxygen.

mg of the Mn-complex was the optimal catalyst amount. To demonstrate the effectiveness of the Mn-complex, the model reaction was performed without the catalyst. However, the yield of the model reaction remained below 20% even after a duration of 10 h. To ensure the reliability of the specified event, the model reaction was performed without a catalyst in an air atmosphere. Nevertheless, the yield of the model reaction did not exceed 35% even after a period of 10 h.

Upon obtaining the optimization results, an assessment was conducted to determine the applicability and extent of this approach in the epoxidation of substituted styrenes (Table 10). The data presented in Table 10 reveals that the desired end products were successfully synthesized with yields ranging from 73% to 94% across various alkenes, encompassing both electron-donating and electron-withdrawing substituents. It is worth noting that previous literature reports have indicated the possibility of generating additional by-products, such as aldehydes, carboxylic acids, and alcohols, during the epoxidation process of alkenes [45–47]. The exploration of turnover number (TON) and turnover frequency (TOF) within catalytic systems constitutes a significant area of research. TON is widely recognized as an effective parameter for assessing the rates of organic chemical reactions across various catalysts. In this study, the manganese (Mn) content was determined using atomic absorption spectroscopy, revealing that 250 mg of catalyst corresponds to 2.5 mol% of the catalyst. Consequently, with the mol% of the catalyst established, it becomes feasible to compute the TON and TOF for the Mn-complex. The data presented in the table indicates that the TON and TOF values ranged from 37.6 to 29.2 and from 12.5 to 3.6, respectively. Furthermore, the screening results indicate that the catalyst exhibited inferior performance with aliphatic substrates when compared to styrene derivatives.

3.5 The mechanism of epoxidation of alkenes

In this investigation, we suggest that the potential mechanism underlying the formation of epoxides from alkenes involves the reaction of sodium periodate and water in the presence of a manganese catalyst, resulting in the formation of the [Mn(II)Ligand-HOOH] adduct. The deprotonation of this adduct yields the [Mn(II)Ligand-OOH] intermediate, which is subsequently transformed into the Mn(IV)=O intermediate that facilitates the transfer of oxygen to the olefin. The heterolytic cleavage of the O-O bond within the hydroperoxo intermediate, activated by the catalyst, generates the oxo-species [Ligand-Mn(IV)=O], which then transfers oxygen to the olefin. This proposed mechanism bears resemblance to that suggested by Rocha et al. [54].

3.6 Investigation of catalyst reusability

The ability to reuse the Mn-catalyst holds significant value from both synthetic and economic perspectives in this original research. Remarkably, the homogeneous [Mn(II)-Ligand] can be recovered up to four times, with minimal

Table 10. Application of Mn-complex in epoxidation of alkenes in the presence of sodium periodate.

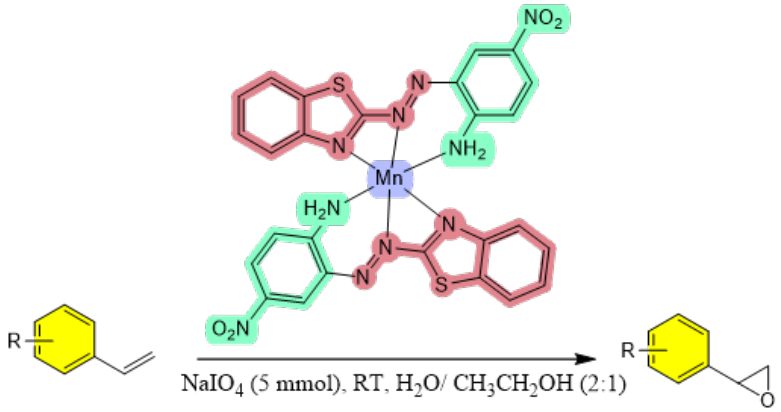

Entry	Substrate	Product	Conversion (%)	Time (h)	Yield (%)	TON	TOF (h^{-1})
1	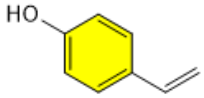	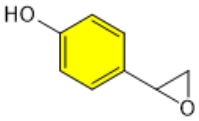	100	3.0	92	36.8	12.3
2	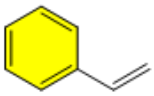	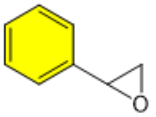	99	3.5	87	34.8	9.9
3	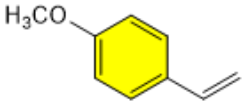	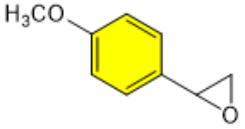	98	3.0	94	37.6	12.5
4	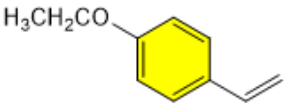	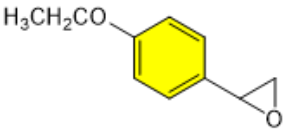	98	3.0	93	37.2	12.4
5	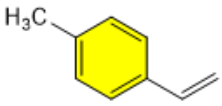	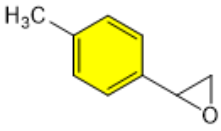	99	4.0	90	36.0	9.0
6	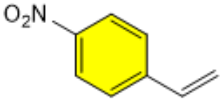	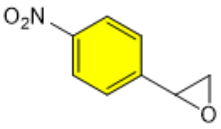	97	6.0	87	34.8	5.8
7	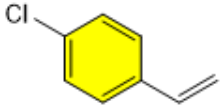	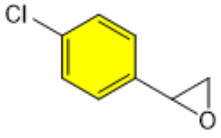	98	6.0	86	34.4	5.7
8	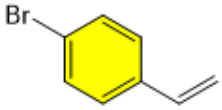	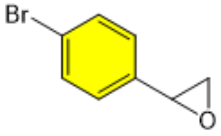	98	6.0	84	33.6	56
9		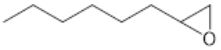	76	8.0	79	31.6	3.9
10		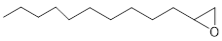	70	8.0	73	29.2	3.6

a)General reaction parameters: Substrate (5 mmol)/(2.5 mol%), $NaIO_4$ (5 mmol), Room temperature, Mn-complex (250 mg), Solvent (H_2O: CH_3CH_2OH) (2:1) (10 mL), b) GC yield based on the starting material.

loss of activity observed. The reusability of [Mn(II)-Ligand] was examined through multiple sequential epoxidation reactions of 4-hydroxystyrene using $NaIO_4$ in both water and ethanol. After each reaction, the catalyst was separated from the reaction mixture by simple filtration, followed by washing with a diethyl ether and chloroform mixture, and subsequently dried to prepare for the next reaction cycle. Upon utilizing the catalyst for four successive cycles, the epoxide yields were recorded as 92%, 89%, 87%, and 84%, corresponding to nearly 100% conversion in the first, second, third, and fourth catalytic cycles, respectively (Table 11). The filtrates were gathered for the assessment of manganese leaching. The findings revealed that during the initial four runs, manganese was not significantly detected in the filtrates through atomic absorption spectrometry. The characteristics of the recovered catalysts were monitored using infrared spectroscopy. The results demonstrated that the [Mn(II)-Ligand] catalysts exhibited no alterations in their infrared spectra after multiple reuse cycles.

3.7 A comparison study for thermal method

To demonstrate the advantages and effectiveness of the current methodology for the epoxidation of alkenes, we conducted a comparative analysis of the epoxidation of styrene against findings from various scientific studies documented in the literature (see Table 12). The results obtained indicate that the newly developed method is beneficial regarding the quantity of catalyst used, the reaction temperature, and the reusability of the homogeneous manganese catalyst.

3.8 Investigation of catalytic efficiency of Mn-complex under microwave irradiations

In our investigation of the epoxidation of styrene, we focused on the oxidation process utilizing sodium periodate in conjunction with a catalytic quantity of manganese complex. This approach served as a straightforward model reaction conducted under microwave irradiation. We systematically varied several reaction parameters, including the amount of catalyst, the choice of solvent, the microwave power, and the reaction temperature, as detailed in Table 13. Selecting a suitable solvent is of paramount significance for the effective implementation of microwave-assisted organic synthesis. To identify the most effective solvents, the model reaction was conducted in various solvents, including water, ethanol (EtOH), acetonitrile (CH_3CN), and dichloromethane, as detailed in Table 13, entries 1-4. As indicated in Table 13, entry 4 yielded the most favorable outcome for the reaction medium of the model. Consequently, CH_2Cl_2 was selected as the solvent for the reaction. Furthermore, we investigated the model reaction utilizing varying quantities of the catalyst (refer to Table 13, entries 5-6). The optimal outcome was achieved with 100 mg of the manganese complex. To optimize the power settings of a microwave oven, a reduction in power from 250 W to 200 W resulted in an extended duration for the model reaction and a decrease in the yields of the target products. At a power level of 300 W, the yield and reaction time were recorded at 50% and 3 minutes, respectively. The elevated power settings of the microwave oven caused significant charring of the desired product (refer to Table 13, entries 7-8). The optimization of the microwave oven temperature was conducted at three specific settings: 60, 70, and 80 °C (refer to Table 13, entries 9-10). The results indicate that the optimal temperature for the process was determined to be 70 °C.

Table 14 illustrates the utilization of various aromatic and aliphatic alkenes to demonstrate the effectiveness and advantages of this method in the epoxidation process. To establish generalized optimal reaction conditions, several styrene derivatives were tested with a catalytic quantity of Mn-complex (100 mg or 1 mol%) at a power setting of 250 W and a temperature of 70 °C under microwave irra-

Table 11. Screening the reusability of Mn(II)-Ligand catalyst[a].

Run	Yield (%)[b]	Leached Mn (%)[c]
1	92	0.8
2	89	0.05
3	87	Trace
4	84	0

a) Reaction conditions: 4-hydroxystyrene (5 mmol), $NaIO_4$ (5 mmol), Room temperature, Mn-complex (250 mg), Solvent (H_2O: CH_3CH_2OH) (2:1) (10 mL). b) GC Yields. c) The leaching of metal determined by atomic absorption spectroscopy (AAS).

Table 12. Screening the reusability of Mn(II)-Ligand catalyst[a].

Entry	Catalyst name	Amount of catalyst	T (°C)	Time (h)	Yield (%)	Ref.
1	MCM-41@CP@PAL@Cu	8.5 mol%	100	1.5	82	[48]
2	V_2O_5/$FeVO_4$	11 mol%	90	2.5	87	[49]
3	Vanadium Schiff base	10 mol%	75	4	88	[50]
4	Cu/Co-Co PBA-250	12 mol%	250	3	89	[51]
5	MnL1-MnL7	8 mol%	100	4	90	[52]
6	Cr-complex	5 mol%	RT	2.5	89	[53]
7	Mn-complex	2.5 mol%	RT	3.5	87	This work

Table 13. Optimization of the reaction conditions under microwave irradiations [a].

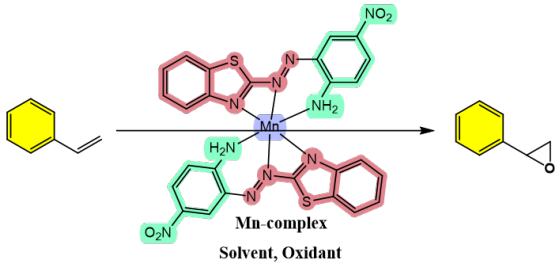

Entry	Catalyst (mg)	Solvent	Power (w)	T (°C)	Time (h)	Yield (%)[b]
1	100	H_2O	250	70	5	45
2	100	EtOH	250	70	5	60
3	100	CH_3CN	250	70	5	50
4	100	CH_2Cl_2	250	70	3	95
5	90	CH_2Cl_2	250	70	3	90
6	110	CH_2Cl_2	250	70	3	93
7	100	CH_2Cl_2	200	70	6	60
8	100	CH_2Cl_2	300	70	3	50
9	100	CH_2Cl_2	250	60	10	50
10	100	CH_2Cl_2	250	80	3	95

a) General reaction conditions for microwave irradiation: styrene (2 mmol), sodium periodate (2 mmol), Mn-complex (x mg), solvent (10 mL), power of microwave (y W). b) monitoring using GC.

Table 14. Generality and versatility of microwave irradiations for epoxidation of alkenes [a].

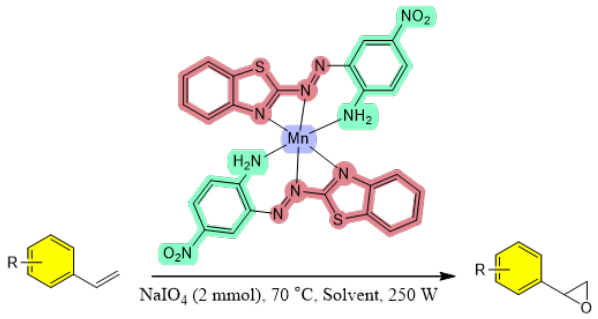

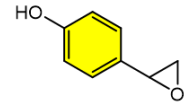

Yield: 94%, Time: 3 min. TON: 94, TOF(h^{-1}): 1880

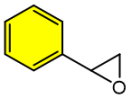

Yield: 95%, Time: 3 min. TON: 95, TOF(h^{-1}): 1900

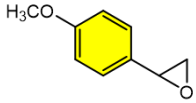

Yield: 96%, Time: 4 min. TON: 96, TOF(h^{-1}): 1432

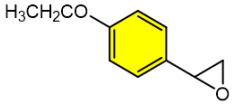

Yield: 91%, Time: 5 min. TON: 91, TOF(h^{-1}): 1096

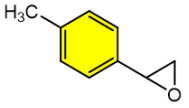

Yield:90%, Time: 3 min. TON: 90, TOF(h^{-1}): 1800

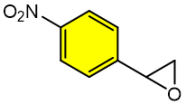

Yield: 90%, Time: 5 min. TON: 90, TOF(h^{-1}): 1084

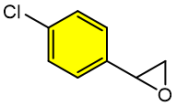

Yield: 89%, Time: 6 min. TON: 89, TOF(h^{-1}): 890

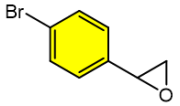

Yield: 89%, Time: 6 min. TON: 89, TOF(h^{-1}): 890

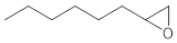

Yield: 89%, Time: 7 min. TON: 89, TOF(h^{-1}): 742

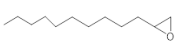

Yield: 90%, Time: 6 min. TON: 90, TOF(h^{-1}): 900

a) General reaction conditions: alkene (2 mmol), $NaIO_4$ (2 mmol), catalyst (100 mg/ 1 mol%), CH_2Cl_2 (10 mL), T: 70 °C, Power: 250 w.

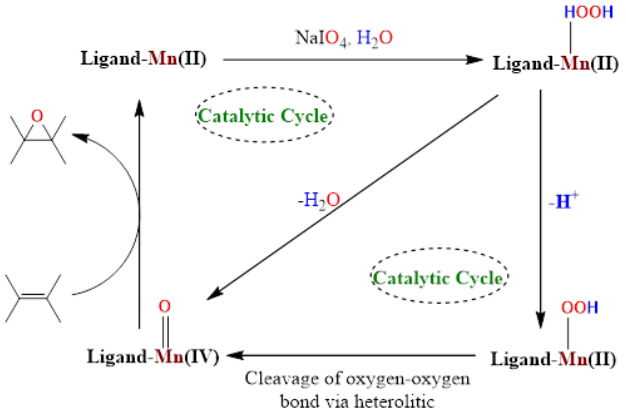

Scheme 3. A reasonable mechanism for the epoxidation of alkenes with sodium periodate in the presence of Mn (II)-Ligand.

diation. The reaction progressed efficiently, yielding the desired epoxides in high yields and reduced reaction times compared to traditional thermal methods. It is noteworthy that our observations indicated that two aliphatic alkenes exhibited moderate yields and prolonged reaction times under thermal conditions. In contrast, when subjected to microwave irradiation, both the yield and reaction time demonstrated significantly improved performance compared to the thermal conditions.

4. Conclusion

The complexes in this study were synthesized by reacting the ionic metal with the ligand derived from azo. Characterization of these compounds was carried out using techniques such as melting point analysis, spectroscopy, conductivity measurements, and magnetic susceptibility studies. Moreover, the antimicrobial activity of these complexes against microorganisms external to the experimental system was investigated. Based on the results obtained, the geometric structure of the octahedral complexes that were synthesized was proposed. Additionally, the efficiency of a Mn-complex catalyst in the epoxidation of substituted styrenes was assessed (scheme 3).

Availability of data and materials
The data that support the findings of this study are available from the corresponding author, upon reasonable request.

Conflict of interests
The author declare that they have no known competing financial interests or personal relationships that could have appeared to influence the work reported in this paper.

References

[1] S. Bilgen. *Renewable and Sustainable Energy Reviews*, **38**(2014): 890–902.
DOI: https://doi.org/10.1016/j.rser.2014.07.004.

[2] A. Al-Ghandoor, J. O. Jaber, I. Al-Hinti, and I. M. Mansour. *Renewable and Sustainable Energy Reviews*, **13**(2009).
DOI: https://doi.org/10.1016/j.rser.2008.09.008.

[3] J. Muzart. *Synthesis*, **1995**(1995):1325–1347.
DOI: https://doi.org/10.1055/s-1995-4128.

[4] S. Jin Choi, U. Sang Shin, and S. H. Kim. *Tetrahedron Lett.*, **117**(2023):154378.
DOI: https://doi.org/10.1016/j.tetlet.2023.154378.

[5] B. R. Moser, S. C. Cermak, K. M. Doll, J. A. Kenar, and B. K. Sharma. *J. Am. Oil Chem. Soc.*, **99**(2022):801–842.
DOI: https://doi.org/10.1002/aocs.12623.

[6] S. Verma, A. Joshi, S. R. De, and J. L. Jat. *New J. Chem.*, **46**(2022): 2005–2027.
DOI: https://doi.org/10.1039/D1NJ04950J.

[7] T. Maharana, N. Nath, H. C. Pradhan, S. Mantri, A. Routaray, and A. K. Sutar. *React. Funct. Polym.*, **171**(2022):105142.
DOI: https://doi.org/10.1016/j.reactfunctpolym.2021.105142.

[8] A. A. Ryan, S. D. Dempsey, M. Smyth, K. Fahey, T. S. Moody, S. Wharry, P. Dingwall, D. W. Rooney, J. M. Thompson, P. C. Knipe, and M. J. Muldoon. *Org. Process Res. Dev.*, **27**(2023):262–268.
DOI: https://doi.org/10.1021/acs.oprd.2c00222.

[9] Z. Yan, J. Tian, K. Wang, K. D. P. Nigam, and G. Luo. *Chem. Eng. Sci.*, **229**(2021):116071, .
DOI: https://doi.org/10.1016/j.ces.2020.116071.

[10] M. R. Elsby and R. T. Baker. *Chem. Soc. Rev.*, **49**(2020):8933–8987.
DOI: https://doi.org/10.1039/D0CS00509F.

[11] N. W. Kinzel, C. Werlé, and W. Leitner. *Angew. Chem. Int. Ed.*, **60**(2021):11628–11686.
DOI: https://doi.org/10.1002/anie.202006988.

[12] X. Liu, Z. Chen, S. Xu, G. Liu, Y. Zhu, X. Yu, L. Sun, and F. Li. *J. Am. Chem. Soc.*, **144**(2022):19770–19777, .
DOI: https://doi.org/10.1021/jacs.2c06273.

[13] M. L. Mohammed and B. Saha. *Energies*, **15**(2022):2858.

[14] I. Triandafillidi, M. G. Kokotou, D. Lotter, C. Sparr, and C. G. Kokotos. *Chem. Sci.*, **12**(2021):10191–10196.
DOI: https://doi.org/10.1039/D1SC02360H.

[15] M. Porchia, M. Pellei, F. Del Bello, and C. Santini. *Molecules*, **25**(2020):5814.

[16] R. Mondal, A. K. Guin, G. Chakraborty, and N. D. Paul. *Org. Biomol. Chem.*, **20**(2022):296–328.
DOI: https://doi.org/10.1039/D1OB01153G.

[17] Y. Tanabe and Y. Nishibayashi. *Coord. Chem. Rev.*, **472**(2022): 214783.
DOI: https://doi.org/10.1016/j.ccr.2022.214783.

[18] A. Neshat, P. Mastrorilli, and A. Mousavizadeh Mobarakeh. *Molecules*, **27**(2022):95.

[19] F. He, K. P. Zois, D. Tzeli, A. A. Danopoulos, and P. Braunstein. *ord. Chem. Rev.*, **514**(2024):215757, .
DOI: https://doi.org/10.1016/j.ccr.2024.215757.

[20] W. Stroek and M. Albrecht. *Chem. Soc. Rev.*, **53**(2024):6322–6344.
DOI: https://doi.org/10.1039/D4CS00021H.

[21] Q. Yan, X. Wu, H. Jiang, H. Wang, F. Xu, H. Li, H. Zhang, and S. Yang. *Coord. Chem. Rev.*, **502**(2024):215622, .
DOI: https://doi.org/10.1016/j.ccr.2023.215622.

[22] F. P. Guengerich. *Drug Metab. Disposition*, **52**(2024):493–497.
DOI: https://doi.org/10.1124/dmd.123.001431.

[23] O. Skorokhod, E. Vostokova, and G. Gilardi. *BioFactors*, **50**(2024): 16–32.
DOI: https://doi.org/10.1002/biof.1996.

[24] Q. He, M. P. Pu, Z. Jiang, H. Wang, X. Feng, and X. Liu. *J. Am. Chem. Soc.*, **145**(2023):15611–15618, .
DOI: https://doi.org/10.1021/jacs.3c05476.

[25] Y. Zhao, M. Duan, C. Deng, J. Yang, S. Yang, Y. Zhang, H. Sheng, Y. Li, C. Chen, and J. Zhao. *Nature Communications*, **14**(2023): 1943.
DOI: https://doi.org/10.1038/s41467-023-37620-8.

[26] H. Liu, W. Liu, G. Xue, T. Tan, C. Yang, P. An, W. Chen, W. Zhao, T. Fan, C. Cui, Z. Tang, and G. Li. *J. Am. Chem. Soc.*, **145**(2023): 11085–11096, .
DOI: https://doi.org/10.1021/jacs.3c00460.

[27] H. Hu, Y. Li, Y. Li, Y. Ding, Y. Sun, and Y. Li. *J. Catal.*, **421**(2023): 45–54.
DOI: https://doi.org/10.1016/j.jcat.2023.02.016.

[28] V. K. Tyagi and S. L. Lo. *Renewable and Sustainable Energy Reviews*, **18**(2013):288–305.
DOI: https://doi.org/10.1016/j.rser.2012.10.032.

[29] T. Wei, Z. Fan, G. Luo, C. Zheng, and D. Xie. *Carbon*, **47**(2009): 337–339.
DOI: https://doi.org/10.1016/j.carbon.2008.10.013.

[30] H. Naeimi and M. Golestanzadeh. *New J. Chem.*, **39**(2015):2697–2710.
DOI: https://doi.org/10.1039/C4NJ02340D.

[31] Á. Díaz-Ortiz, P. Prieto, and A. de la Hoz. *The Chemical Record*, **19**(2019):85–97.
DOI: https://doi.org/10.1002/tcr.201800059.

[32] A. d. la Hoz, A. Díaz-Ortiz, and A. Moreno. *J. Microw. Power Electromagn. Energy*, **41**(2006):45–66.
DOI: https://doi.org/10.1080/08327823.2006.11688549.

[33] A. de la Hoz, A. Díaz-Ortis, A. Moreno, and F. Langa. *Eur. J. Org. Chem.*, **2000**(2000):3659–3673.
DOI: https://doi.org/10.1002/1099-0690(200011)2000:22<3659::AID-EJOC3659>3.0.CO;2-0.

[34] P. Lidström, J. Tierney, B. Wathey, and J. Westman. *Tetrahedron*, **57**(2001):9225–9283.
DOI: https://doi.org/10.1016/S0040-4020(01)00906-1.

[35] A. M. Jreo. *Anal. Biochem*, **4**(2015):1–5.
DOI: https://doi.org/10.4172/2161-1009.1000167.

[36] G. Iniama, E. Nfor, E. Okon, and I. Iorkpiligh. *Int. J. Sci. Techn. Res.*, **3**(2014):73–77.

[37] H. M. Farhan. *World Science Research Journals*, **2**(2014):26–34.

[38] G. B. Vadher and R. V. Zala. *Int. J. Chem. Sci.*, **9**(2011):87–94.

[39] M. Al-Sheikh, H. Y. Medrasi, K. Usef Sadek, and R. A. Mekheimer. *Molecules*, **19**(2014):2993–3003.

[40] A. J. Jarad and S. H. Quiasim. *J. Pharm. Biol. Chem. Sci.*, **9**(2018): 631–642.

[41] M. Wächtler, J. Guthmuller, L. González, and B. Dietzek. *Coord. Chem. Rev.*, **256**(2012):1479–1508.
DOI: https://doi.org/10.1016/j.ccr.2012.02.004.

[42] J. Malinowski, D. Zych, D. Jacewicz, B. Gawdzik, and J. Drzeżdżon. *International Journal of Molecular Sciences*, **21**(2020):5443.

[43] K. Mostafa MH, I. Eman H, M. Gehad G, Z. Ehab M, and B. Ahmed. *Open Journal of Inorganic Chemistry*, **2012**(2012):1–9.
DOI: https://doi.org/10.4236/ojic.2012.22003.

[44] S. R. Al-Ayash, T. H. Al-Noor, and A. Abdou. *Russ. J. Gen. Chem.*, **93**(2023):987–995.
DOI: https://doi.org/10.1134/S107036322304028X.

[45] H. Pallathadka, H. K. Mohammed, Z. H. Mahmoud, A. A. Ramírez-Coronel, F. M. A. Altalbawy, M. A. Gatea, and M. Kazemnejadi. *Inorg. Chem. Commun.*, **154**(2023):110944.
DOI: https://doi.org/10.1016/j.inoche.2023.110944.

[46] J. Li, W. Gu, Z. Wang, X. Zhou, and Y. Chen. *ChemBioChem*, **24**(2023):e202200719.
DOI: https://doi.org/10.1002/cbic.202200719.

[47] M. Alvear, F. Orabona, K. Eränen, J. Lehtonen, S. Rautiainen, M. Di Serio, V. Russo, and T. Salmi. *Chem. Eng. Sci.*, **269**(2023):118467.
DOI: https://doi.org/10.1016/j.ces.2023.118467.

[48] A. Malik and U. P. Singh. *J. Porous Mater*, **30**(2023):2011–2021.
DOI: https://doi.org/10.1007/s10934-023-01475-7.

[49] J. Liu, W. Wang, L. Wang, and P. Jian. *J. Colloid Interface Sci.*, **630**(2023):804–812, .
DOI: https://doi.org/10.1016/j.jcis.2022.10.076.

[50] C. Salubi. *Current Chemistry Letters*, **12**(2023):91–106.
DOI: https://doi.org/10.5267/j.ccl.2022.9.003.

[51] Y. Fu, L. Liu, S. Tricard, K. Liang, J. Zhang, J. Fang, and J. Zhao. *Appl. Catal. A*, **657**(2023):119161.
DOI: https://doi.org/10.1016/j.apcata.2023.119161.

[52] B. Maleki, R. Sandaroos, and S. Peiman. *Heliyon*, **9**(2023).

[53] R. S. Mahmood, M. I. Abowd, and A. B. Sabti. *Iran. J. Catal.*, **13**(2023).
DOI: https://doi.org/10.30495/ijc.2023.1986079.2007.

[54] M. Rocha, S. L. H. Rebelo, and C. Freire. *Appl. Catal. A.*, (2013): 116–123.
DOI: https://doi.org/10.1016/j.apcata.2013.04.025.